JOURNAL OF BALKAN GEOPHYSICAL SOCIETY, Vol.8, No 3, August 2005, p.74-88

NON-LINEAR INVERSION OF SEISMIC DATA FOR THE DETERMINATION OF REFLECTOR GEOMETRY AND VELOCITY STRUCTURE

Pantelis M. Soupios[(1)], Constantinos B. Papazachos[(2)], Gregory N. Tsokas[(2)], Antonis Vafidis[(3)]

(1) Laboratory of Geophysics & Seismology, Department of Natural Resources and Environment, Technological Educational Institute of Crete, Chania, Greece
(2) Geophysical Laboratory, Aristotle University of Thessaloniki, P.O. Box 352-1 54006, Macedonia, Greece
(3) Applied Geophysics Laboratory, Department of Mineral Resources Engineering, Technical, University of Crete, Chania, Greece

Abstract: *A nonlinear method is used to compute first seismic arrivals and reflection travel times for velocity models with complex reflector geometry. The method uses a combination of refraction and reflection travel-times for simultaneous determination of velocity and interface depth of the model. The elastic waves assumed to be transmitted or reflected at interfaces at which the raypaths satisfy Snell's law. The travel times of critically refracted waves and derivative matrix are computed by applying a revised ray bending method, supplemented by an approximate computation of the first Fresnel zone at each point of the ray. Travel-times and raypaths of reflected waves are computed by applying a fast finite-difference scheme based on a solution to the eikonal equation and following the travel-time gradient backward from the receiver to the source, respectively.*

A damped least squares inversion scheme is used to reconstruct the velocity model above the reflector and the geometry of the interface by minimizing the difference between observed and calculated (direct, refracted and reflected) travel-times. In order to reduce inversion artifacts both damping and smoothing regularization factors are applied. The applicability of the proposed method is tested using synthetic data. This simultaneous inversion scheme is appropriate for static seismic corrections, as well as determination of lateral velocity variations and reflector's geometry.

INTRODUCTION

Travel-time tomography is primarily used by seismologists to study the 3-D velocity variation in the upper crust (e.g Papazachos and Nolet, 1997). This method was first introduced by Aki, Christofferson and Husebye (1977) who divided a horizontally layered media into a Cartesian grid of cells with values of slowness assigned at each cell and calculated the slowness distribution by inverting the observed travel times. The next step was the application of the same method in problems with two types of unknown parameters, such as, the earthquake parameters and the velocity structure (e.g Aki and Lee, 1976; Thurber, 1983).

The tomography method of Aki et al. (1977) was adapted to reflection data by Bishop et al. (1985) and Farra and Madariaga (1988). Reflection tomography has been used for seismic data analysis primarily by petroleum companies, processing a large number of recordings for different source - receiver location to estimate the sub-surface velocity structure and reflector location. Until very recently, applications of travel-time inversion methods to these two different types of data (first breaks and reflection travel-times) had been carried out

independently. Recently, refraction and reflection data have been processed simultaneously in order to obtain a better knowledge of the study area (Zhang et. al., 1998; Zelt et. al., 1999) by applying simultaneous seismic refraction and reflection tomography for determination of shallow and/or deep velocity and interface structure. In reflection tomography, we can parameterise the reflector and velocity field in some suitable fashion and simultaneously invert them. This approach is very attractive since it treats both inversion parameters on the same basis (Bishop et al., 1985; Farra and Madariaga, 1988; Hobro et al., 2003; Trinks et al., 2005). However, because of the trade-off between media velocity and reflector depth (the velocity-depth ambiguity e.g Stork and Clayton, 1986; Bickel, 1990; Lines, 1993; Ross, 1994; Tieman, 1994) the reflector interfaces and velocity cannot be uniquely determined without a priori information on reflector location.

It is well known that refraction tomography provides better long-wavelength velocity information, with no or very little control on the configuration of reflecting interfaces. Therefore, if both refraction and reflection data (wide-angle, normal-incidence) are available along a profile, simultaneous inversion of both datasets can provide better control on both velocity and reflector's geometry.

In the present study we examine possible improvements of the standard simultaneous tomography using ray theory. For the travel times of the critically refracted waves we follow the approach developed in a previous work (Soupios et al., 2001). Specifically, initial rays are calculated using a fast, approximate ray tracing method, known as the ray initializer (Thurber and Ellsworth, 1980), which is equivalent to solving a one-dimensional approximation to the actual three-dimensional problem. This method provides an initial estimate of the minimum-time ray paths in heterogeneous media for the final ray tracing with a revised ray bending technique (Moser et al., 1992). Moreover, knowing, that the properties of the ray are influenced not only by the structure along the ray, but also by the structure in some "vicinity" of the ray, we incorporate physical rays by estimating the approximate width of first Fresnel volume which is frequency dependent (Cerveny and Soares, 1992, Woodward, 1992).

The travel-times of the reflected waves are computed by a finite-difference algorithm which incorporates propagation of waves in complex velocity models (Hole and Zelt 1995). Snell's law for reflections is used in the vicinity of the reflecting interface. The reflector model is allowed to vary smoothly with depth, which means that the depth to the interface $d_{i,k}$ could take any real value and it is not constrained to lie at grid nodes. The advantage of this method is that travel-times are computed simultaneously for all receivers. The raypaths and the depth derivatives are stored in order to construct the derivative matrix. A continuous reflector is also used and represented by a series of support points whose depth varies as function of horizontal offset. Rays are traced backward in time from receiver locations down to reflecting interfaces and then back up to source locations to determine the expected travel-times (forward modeling). The result is a system of linear equations consisting of two types of parameters, corresponding to slowness and reflector depth.

It is generally assumed (Anderson et. al., 1984) that the inversion problem is overdetermined and hence, can be solved in a least-squares sense by minimizing the data misfit. Since there is frequently a

certain degree of non-uniqueness or ill conditioning in the problem, the standard approach is to construct a "least-structure" solution (Franklin, 1970; Tarantola and Nercessian, 1984; Constable et al., 1987) by considering additional constraints and usually minimizing the model and/or one of the model derivative norms. The inverse problem is solved by either the Levenberg-Marquardt (L-M) method (also known as the damped least squares method-Levenberg, 1944; Marquardt, 1963), or by using both a damping factor and a roughness term, in the form of e.g. a second derivative smoothing filter to the slowness model (Constable et al., 1987).

To show the efficiency of our algorithm, we consider three problems: first, we invert travel-times to solve only for the velocity structure, then we invert first arrivals and reflection travel-times to determine only the geometry of the optimum reflector and finally we used the travel-times to simultaneously solve for depth and velocity structure. We apply the method using 3D synthetic data. The proposed algorithm is useful for shallow seismic surveys (Soupios, 2002) as well as, in the determination of deeper structures depending on the scale of the problem.

FORWARD MODELING

Model parameterization

In local inversion studies, a flat layered Earth model is commonly used (Aki and Lee, 1976). A similar assumption was also adopted here because of the small scale of our study area and the convenience of the cartesian coordinate system, which significantly speeds up all computations, especially those concerning the 3-D ray tracing. Our model is composed of a three-dimensional (3-D) grid of blocks of same size, with values of slowness assigned at the grid points. The slowness at a point which is located between nodes 1 to 8 is calculated by trilinear interpolation, as given by the following equation,

$$\text{slowness}=wfz_2*(wfy_2*(wfx_2*n1+wfx_1*n2)+wfy_1*(wfx_2*n3+wfx_1*n4))+ wfz1*(wfy2*(wfx2*n5+wfx1*n6)+wfy1*(wfx2*n7+wfx1*n8)) \quad (1)$$

where n1,n2,…,n8 denote the slowness values at the nodes of the grid block and $wf(x,y,z)_{1,2}$ are the weights. Either smooth velocity models or models with velocity discontinuities can be easily used (Hole and Zelt, 1995). We also incorporated a velocity discontinuity interface, which is defined by a set of points “connected” by trilinear interpolation. The main advantage of the method is that the reflector can be located anywhere in the model (Hole and Zelt, 1995) and not necessarily lie on the slowness grid nodes.

Ray Tracing

The successful solution of the forward modelling involves the accurate calculation of the travel-times for the two types of waves (refracted and reflected) and the estimation of the partial derivatives of the travel-times with respect to both velocity and depth at the nodes (based on the starting velocity and reflector model).

Rays for the first arrivals are calculated using a revised bending algorithm (Moser et al., 1992), which has superior convergence properties. In an effort to alleviate problems such as convergence and execution speed associated with the bending method, we incorporated the approximate ray tracing scheme of Thurber and Ellsworth (1980). In this approach, an equivalent one-dimensional (1-D) structure is calculated from the 3-D model between each source-receiver pair. The velocities at the grid points

that fall within the model are harmonically averaged, which is equivalent to arithmetically averaging the slowness. These average values are used as layer velocities for the one-dimensional model, where the direct and all possible refracted waves are considered. The direct ray is determined using a combination of the false position method and the secant method (Press et al., 1988), while refracted rays are handled using time terms (Officer, 1958). The minimum travel-time path from this ray tracing routine is used as the initial ray path guess for our bending ray tracing routine (Moser et al., 1992). In this technique the ray is represented by a series of support points which describe the ray path with the use of Beta-splines (Pereyra, 1992). The travel time along the Beta-spline curve can be calculated with the trapezoidal rule. Finally, we defined the width of the approximate Fresnel volume for each point along the raypath from the source to the receiver, as suggested by Soupios et al. (2001).

The first Fresnel is incorporated by applying a simple algebraic manipulation on the elements of the raypath matrix, M. This operation distributes the value of the matrix elements which correspond to ray points to its Fresnel volume. The implementation of the proposed equation (Soupios et al., 2001), is much more simple for the calculation of the Fresnel volume, since we only need the raypath connecting the given source and receiver and the dominant frequency of our signal for the wavelength estimation.

The ray tracing for the reflected waves is performed using a fast finite difference scheme (Hole and Zelt, 1995). After specifying the velocity model, the travel time of the incident wave to the reflecting interface is first calculated. Since waves that turn at or below the reflector may arrive earlier but surely do not represent the reflected arrival, velocities below the interface are set to be slower than velocities above the reflector (Podvin and Lecomte, 1991). Using Snell's law, reflected travel-times are assigned at the nodes immediately above the reflector. The final reflected travel-time is calculated by adding the travel-time from the reflection point to the receiver, to the one previously calculated. Raypaths are determined and partial derivatives of travel-times (matrix M) are calculated from the pre-calculated reflection traveltimes as well as the velocity field and the reflector geometry (Williamson, 1990). This algorithm has been modified to estimate the derivatives moving backward in time.

INVERSION PROCEDURE

For a two-parameter model including slowness and reflector depths, the travel-time deviation $\boldsymbol{\delta t}$ is given as follow,

$$\begin{pmatrix} \mathbf{M}_{tr}^{s} & 0 \\ \mathbf{M}_{ref}^{s} & \mathbf{M}_{ref}^{z} \end{pmatrix} \cdot \begin{pmatrix} \boldsymbol{\delta s} \\ \boldsymbol{\delta z} \end{pmatrix} = \begin{pmatrix} \boldsymbol{\delta t}_{\mathbf{tr}} \\ \boldsymbol{\delta t}_{\mathbf{ref}} \end{pmatrix} \text{ or,}$$

$$\mathbf{M} \cdot \mathbf{x} = \boldsymbol{\delta t} \qquad (3)$$

where $\mathbf{M}_{tr}^{s}$ and $\mathbf{M}_{ref}^{s}$ are matrices (consisting of slowness partial derivatives) for refracted and reflected waves respectively, and $\mathbf{M}_{ref}^{z}$ is a matrix of depth partial derivatives for reflected waves, $\mathbf{x}$ is the correction vector which contains information about slowness and reflector depth, $\boldsymbol{\delta s}$ and $\boldsymbol{\delta z}$ are the velocity and reflector correction vectors and $\boldsymbol{\delta t}$ is a vector of the difference between calculated and observed travel-times.

The matrix $\mathbf{M}$ of equation (3) consists of the partial derivatives with respect to both parameters (velocity-reflector) that have already been calculated. An important issue is the relative weights of the reflected and

refracted arrivals, as well as the trade-off between the slowness, **δs**, and reflector depth, **δz**, corrections. In the present work we follow the Bayessian approach (e.g. Tarantola, 1987), where equation (3) is written as:

$$\mathbf{C}_d^{-1/2}\cdot\mathbf{M}\cdot\mathbf{C}_m^{1/2}\cdot\mathbf{C}_m^{-1/2}\cdot\mathbf{x}=\mathbf{C}_d^{-1/2}\cdot\boldsymbol{\delta}\mathbf{t}\Rightarrow\mathbf{C}_d^{-1/2}\cdot\mathbf{M}\cdot\mathbf{C}_m^{1/2}\cdot\hat{\mathbf{x}}=\mathbf{C}_d^{-1/2}\cdot\boldsymbol{\delta}\mathbf{t} \quad (4)$$

where $\mathbf{C_d}$ and $\mathbf{C_m}$ are the data and model a priori covariance matrices and $\hat{\mathbf{x}}=\mathbf{C}_x^{-1/2}\mathbf{x}$ are the normalized model perturbations. The objective function that we are effectively minimizing is given below,

$$S=(\delta t-Mx)^T C_d^{-1}(\delta t-Mx)+\gamma(x^T C_m^{-1}x) \quad (5)$$

where, γ is a Lagrangian multiplier which controls the trade-off between the normalized model-norm (measure of the solution **x** length) and the normalized fit between the observed and the calculated data.

We consider the simplest and usually adopted case, where velocity and reflector nodes have independent and constant *a priori* errors, s_v and s_z, respectively, equation (5) can be transformed to:

$$S=(\delta t-Mx)^T C_d^{-1}(\delta t-Mx)+\gamma(s_V^{-2}x_V^T x_V+s_z^{-2}x_z^T x_z) \quad (6)$$

where the perturbation vector **x** has been split into two vectors, $\mathbf{x_v}$ and $\mathbf{x_z}$, each containing the velocity and reflector depth perturbations to be determined. Thus, the model variance is described only by the variance of the reflector depth, s_z^2, and the slowness variance, s_s^2 ($s_s=s_v/v^2$) where s_v^2 is the velocity variance.

Moreover, the data errors can be described by the refraction σ_{tr}, and the reflection, σ_{ref}, travel-time errors. These errors control the relative weighting of the two data types. Hence, in order to control the weight of the two data types (refraction-reflection), we use an additional relative-weight factor, r_w, which is calculated as:

$$r_w=\frac{refraction\_weight}{reflection\_weight}=\frac{1/\sigma_{ref}}{1/\sigma_{tr}}=\frac{\sigma_{tr}}{\sigma_{ref}} \quad (7)$$

If we replace $\mathbf{C_d}$ and $\mathbf{C_m}$ in equation (4) by the corresponding variances we derive the following equation:

$$\frac{1}{\sigma_{tr}}\mathbf{M}_{tr}^{S}\cdot\mathbf{s}_s\frac{\boldsymbol{\delta}\mathbf{s}}{\mathbf{s}_s}+0=\frac{1}{\sigma_{tr}}\boldsymbol{\delta}\mathbf{t}_{tr}$$

$$\frac{1}{\sigma_{ref}}\mathbf{M}_{ref}^{S}\cdot\mathbf{s}_s\frac{\boldsymbol{\delta}\mathbf{s}}{\mathbf{s}_s}+\frac{1}{\sigma_{ref}}\mathbf{M}_{ref}^{z}\cdot\mathbf{s}_z\frac{\boldsymbol{\delta}\mathbf{z}}{\mathbf{s}_z}=\frac{1}{\sigma_{ref}}\boldsymbol{\delta}\mathbf{t}_{ref} \quad (8)$$

where $\boldsymbol{\delta}\mathbf{t}$ contains the travel-time residuals, $\mathbf{M}_{tr}^{s}$, $\mathbf{M}_{ref}^{s}$ and $\mathbf{M}_{ref}^{z}$ are slowness and reflector derivative matrices. If we multiply equation (8) with σ_{tr} and use equation (7), we rewrite equation (8) in matrix notation as follows,

$$\overline{\mathbf{M}}\cdot\hat{\mathbf{x}}=\hat{\boldsymbol{\delta}\mathbf{t}} \quad (9)$$

where,

$$\left[\begin{array}{cccc|cccc}
\frac{\partial t_1^{tr}}{\partial s_1}\cdot s_s & \frac{\partial t_1^{tr}}{\partial s_2}\cdot s_s & \cdots & \frac{\partial t_1^{tr}}{\partial s_n}\cdot s_s & 0 & 0 & \cdots & 0\\
\vdots & \vdots & \ddots & \vdots & \vdots & \vdots & \ddots & \vdots\\
\frac{\partial t_K^{tr}}{\partial s_1}\cdot s_s & \frac{\partial t_K^{tr}}{\partial s_2}\cdot s_s & \cdots & \frac{\partial t_K^{tr}}{\partial s_n}\cdot s_s & 0 & 0 & \cdots & 0\\
\frac{\partial t_1^{ref}}{\partial s_1}\cdot s_s r_w & \frac{\partial t_1^{ref}}{\partial s_2}\cdot s_s r_w & \cdots & \frac{\partial t_1^{ref}}{\partial s_n}\cdot s_s r_w & \frac{\partial t_1^{ref}}{\partial z_1}\cdot s_z r_w & \frac{\partial t_1^{ref}}{\partial z_2}\cdot s_z r_w & \cdots & \frac{\partial t_1^{ref}}{\partial z_m}\cdot s_z r_w\\
\vdots & \vdots & \ddots & \vdots & \vdots & \vdots & \ddots & \vdots\\
\frac{\partial t_L^{ref}}{\partial s_1}\cdot s_s r_w & \frac{\partial t_L^{ref}}{\partial s_2}\cdot s_s r_w & \cdots & \frac{\partial t_L^{ref}}{\partial s_n}\cdot s_s r_w & \frac{\partial t_L^{ref}}{\partial z_1}\cdot s_z r_w & \frac{\partial t_L^{ref}}{\partial z_2}\cdot s_z r_w & \cdots & \frac{\partial t_L^{ref}}{\partial z_m}\cdot s_z r_w
\end{array}\right]=\overline{\mathbf{M}}$$

$$\begin{bmatrix} \hat{s}_1 \\ \hat{s}_2 \\ \vdots \\ \hat{s}_n \\ \hline \hat{z}_1 \\ \hat{z}_2 \\ \vdots \\ \hat{z}_m \end{bmatrix} = \hat{\mathbf{x}}, \qquad \begin{bmatrix} \delta t_1^{tr} \\ \delta t_2^{tr} \\ \vdots \\ \delta t_K^{tr} \\ \hline \delta t_1^{ref} . r_w \\ \delta t_2^{ref} . r_w \\ \vdots \\ \delta t_L^{ref} . r_w \end{bmatrix} = \hat{\boldsymbol{\delta}}\mathbf{t} \tag{10}$$

(11)

where m is the number of reflector nodes, n is the number of slowness nodes, K is the number of refraction travel-times, L is the number of reflection travel-times and $\hat{\mathbf{s}}$ and $\hat{\mathbf{z}}$ denote the normalized (with respect to standard error) perturbations of slowness and reflector depth, respectively.

In the current work we present results using the LSQR algorithm originally proposed by Paige and Saunders (1982). The algorithm based on a bidiagonalization of the system using Lanczos method (Lanczos, 1950), followed by a QR decomposition to find the solution.

In order to speed up convergence and stabilize the inversion several approaches can be adopted, as previously described, such as "damping" or "smoothing". In the present work we smooth the slowness perturbations using an appropriate Laplacian operator (Lees and Crosson, 1989) and the reflector geometry by a second-order difference operator (Ammon and Vidale, 1990). The Laplacian operator adds the following system of equations to the travel time inversion problem,

$$-\nabla^2 \hat{s} = \frac{\left(6 \cdot \hat{s}_{i,j,k} - \hat{s}_{i-1,j,k} - \hat{s}_{i+1,j,k} - \hat{s}_{i,j-1,k} - \hat{s}_{i,j+1,k} - \hat{s}_{i,j,k-1} - \hat{s}_{i,j,k+1}\right)}{d^2} = 0 \tag{12}$$

where $\hat{s}_{i,j,k}$ is the normalized slowness perturbation at the (i,j,k) node and d is the grid spacing.

Similarly the second-difference operator adds the system of equations,

$$\nabla^2 \hat{z} = 4 \cdot \hat{z}_{i,j} - \hat{z}_{i-1,j} - \hat{z}_{i+1,j} - \hat{z}_{i,j-1} - \hat{z}_{i,j+1} = 0 \tag{13}$$

where the $\hat{z}_{i,j}$ indicate the reflector depth perturbation at the (i,j) horizontal position.

In order to use the above equations in 2-D problems, we simply reformulate them as, $4 \cdot \hat{s}_{i,k} - \hat{s}_{i-1,k} - \hat{s}_{i+1,k} - \hat{s}_{i,k-1} - \hat{s}_{i,k+1} = 0$ and $2 \cdot \hat{z}_i - \hat{z}_{i-1} - \hat{z}_{i+1} = 0$, respectively.

Moreover, in most cases the derivative matrix has small singular values and is typically highly ill-conditioned. One approach in dealing with this is to use damping factors and augment the system of equations by a set of additional constraints. Since, we are using normalized variables, we can simply write these constrains as $\varepsilon_{s/z} I_{n/m}$ where ε is the damping value, I is the unit matrix and the indices s or z refer to slowness or reflector depth. Typically, ε should be set to 1 (Franklin, 1970) [or σ_{tr} in our case since the system (8) was multiplied by σ_{tr} to define system (9)], if *a priori* data and model errors are correct. Usually ε is set to values higher than 1 to account for outliers, not expected by the Gaussian distribution.

The final augmented system of equations can be written as,

$$\begin{bmatrix} & \overline{M} & \\ \varepsilon_s I_n & | & 0 \\ 0 & | & \varepsilon_z I_m \\ \lambda_s S & | & 0 \\ 0 & | & \lambda_z D \end{bmatrix} \cdot \begin{bmatrix} \hat{s} \\ \hat{z} \end{bmatrix} = \begin{bmatrix} \hat{\delta t} \\ 0 \\ 0 \\ 0 \\ 0 \end{bmatrix} \tag{14}$$

where ε_s and ε_z are the damping factors, λ_s and λ_z are the smoothing factors (concerning slowness and reflector respectively), **S** is the Laplacian operator (equation 12) and **D** is the second difference operator (equation 13).

NUMERICAL EXAMPLE

In order to demonstrate the effectiveness of the proposed technique we have tested our algorithm using four models. In these tests we selected a specific velocity model for the study area and solved the forward problem. Then, the synthetic refracted and reflected travel-times are inverted back to a velocity structure and a specific reflector. Since our synthetic data are error-free we expect that the input (synthetic) model should be recovered. Hence, comparison of the original velocity and what our algorithm recovers permits us to analyse the efficiency of the inversion scheme.

Trying to choose the proper regularization parameters we used the Picard condition and the L-curve criterion as presented by Soupios et al. (2001). Thus, for all the tests described in this section, we conclude that a set of values of λ_s=5.0 and λ_{ref}=3.0 (λ_s and λ_{ref} are described above) should be selected for the final solution since our synthetic data were error free. Also, a similar value ε=5.0 was used for the damping factor.

In the present work we have tested our method for the following cases:

- Assuming that reflector is completely defined by *a priori* information, thus we invert only for the velocity field,
- Assuming that velocity field is completely defined by *a priori* information (velocity analysis etc.), thus we invert only for reflector geometry and,
- Simultaneous determination of the velocity model including the reflector geometry.
- A synthetic test with 3-D source-receiver geometry for a complex geological structure (anticline).

Reconstruction of velocity model

The starting model consists of a four-layer background velocity model where the velocity increases linearly with depth according to the following gradient and table (1):

$$0.075 Km/s \diagup Km \quad (15)$$

and a flat reflector at a depth of 70 Km (figure 1). Model A has a high velocity block (+20%) at depths from 20 to 40 Km. For the next model (B) we used a low velocity anomaly in the same region and with the same amplitude (-20%). In the last model (C), two velocity anomalies (positive and negative) were used. A grid with 41 nodes in the x direction, 1 in the y direction and 21 in the z direction (depth), resulted in a total of 861 velocity nodes (figure 1). For the test we used 19 sources with 10 Km shot spacing and 20 geophones with geophone spacing 10 Km, resulting in 2*380 rays (direct, refracted and reflected waves). For these rays, synthetic travel times were calculated. In the inversion we set the r_w parameter to a minimum (near zero) value in order to calculate the velocity field mainly from the refracted waves.

Figure (1) shows the raypath coverage of the refracted and reflected waves for the study area. The traces of the raypaths of refracted waves are shown by the dotted lines travelling through the model. Reflected raypaths are presented by the dots on the grid lines as the intersection of the raypaths with the grid.

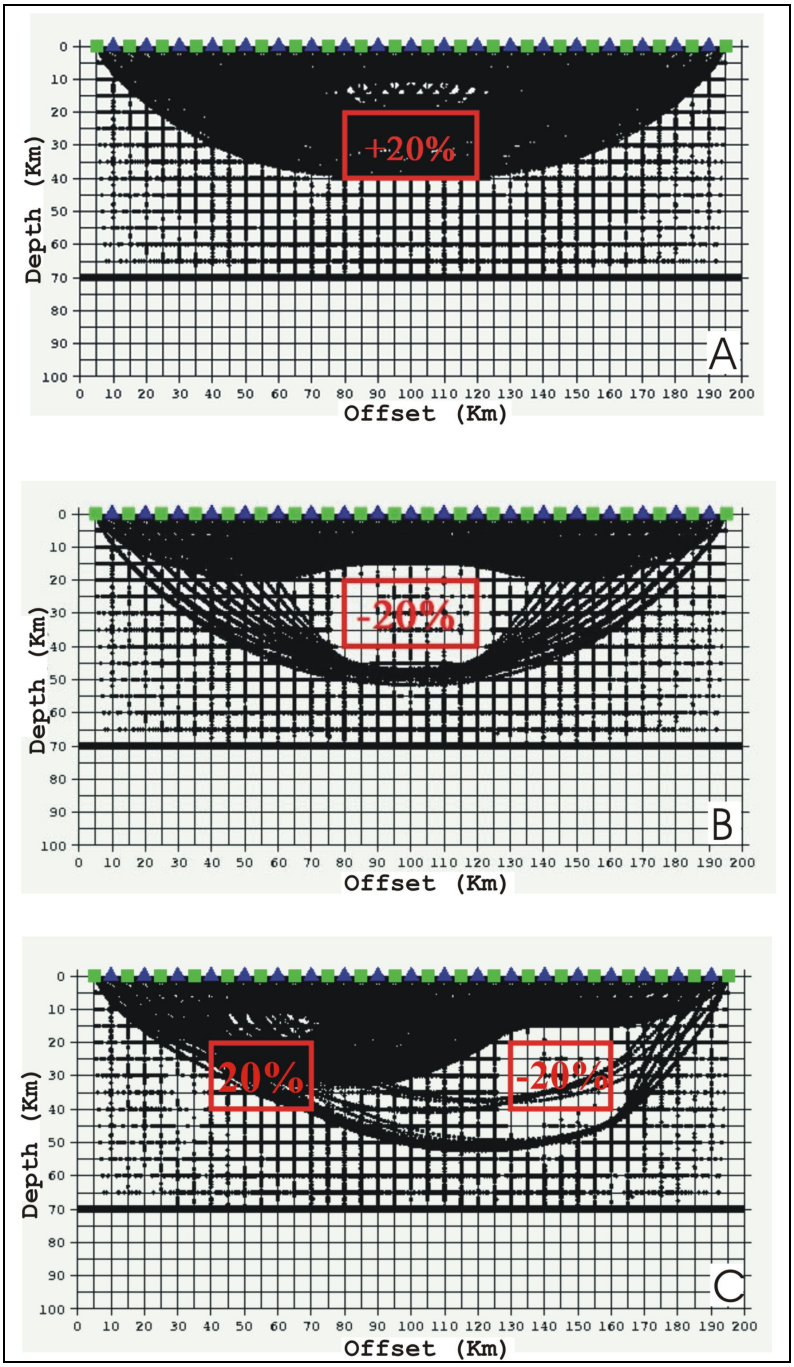

Figure 1. Source-Receiver geometry and the velocity distribution used for the synthetic tests. Ray coverage corresponding to three (A, B & C) different velocity models. The rectangular blocks define the region of velocity anomaly, which referred to the background velocity that increases with depth. The refracted raypaths travelling through the model from and to the surface are also defined. The black traces on the grid lines represent the intersection of the raypath of reflected waves with the model grid. It is obvious that the raypaths "recognize" the existence of the velocity anomalies.

Figure (2) shows the final models from the optimisation-inverse process. The contours represent the percentage (%) of the velocity anomaly compared to the background velocity model. The high velocity rectangular zone is reconstructed quite well.

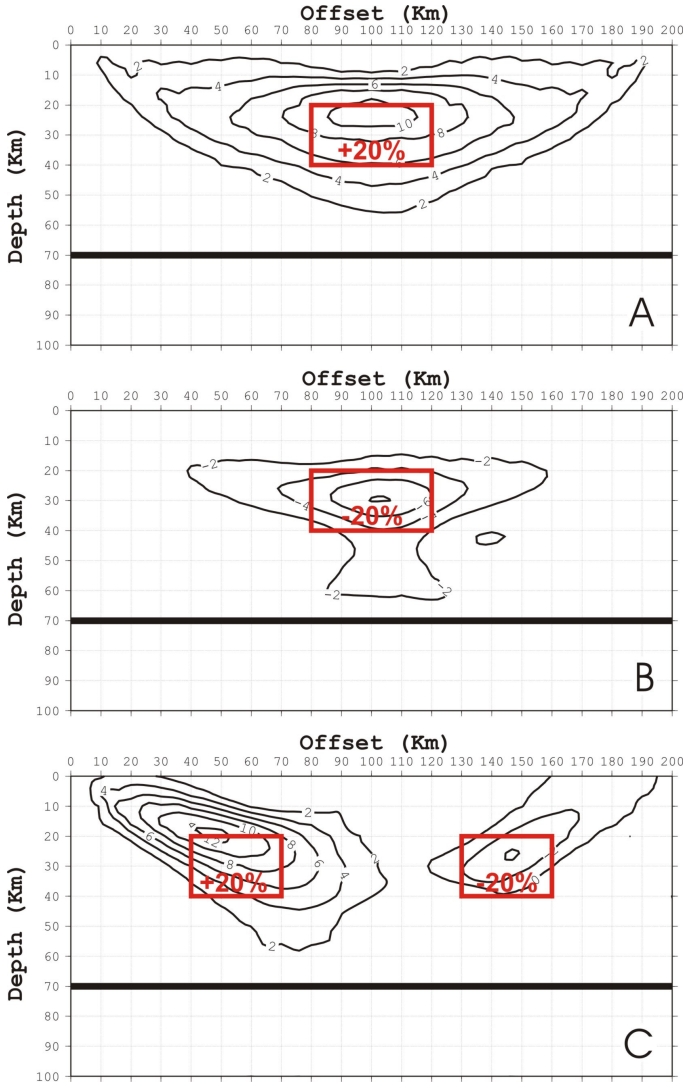

Figure 2. Cross-section of the final inverted velocity model as calculated from inversion of first arrivals and reflection traveltimes. The contours represent the percent (%) of reconstructed velocity model. The constrained reflector is presented by a solid line at 70 Km. A distortion of the shape of the anomalies is found and its amplitude has been underestimated. A) Positive velocity anomaly is reconstructed quite well (>50%), B) The negative velocity anomaly is poorly identified (<50%) since the ray coverage in the area was poor and C) The amplitude of the high velocity anomaly is better reconstructed than the low velocity anomaly (Wielandt, 1987).

For model A, the shape of the high velocity anomaly contours is influenced by the source - receiver geometry. Within the rectangular block, deviations of 10-14% are observed in the reconstructed model compared to the input model. Higher deviations are observed for models B (12-18%) and C (16-20%), due to poor coverage in those regions (figure 1). The high velocity anomaly is better reconstructed because the ray method works well for positive anomalies but is clearly insufficient in the presence of negative anomalies (Wielandt, 1987).

Reconstruction of reflection interface

Using the same source-receiver geometry but a narrower grid (21 nodes in X, 1 node in Y and 11 nodes in Z) we have inverted the travel-times for

interface geometry assuming that velocity field is a priori known. We used three ideal reflectors (figure 3) with different geometry to check the algorithm efficiency. In all cases, a flat reflector was considered at the depth of 70 Km for the starting model. Thus, we had to invert for 21 unknown reflector node parameters (figure 3). In this test, we maximize the effect of reflection derivatives and minimize the refractions, maximizing the r_w parameter value as referred in the previous test. Thus, only the reflection travel-times calculated for each ideal reflector were the input in the inversion process.

Figure (3) presents the ray coverage from the reflected waves as estimated solving the forward problem with finite differences. Low raypath coverage at the edges of the model (reflector) is observed due to the source/receiver and reflector geometry. The same problem appeared in cases B and C in the area where the reflector exhibits, a syncline and a vertical fault, respectively. Thus, low quality of the reconstructed image is expected in those places.

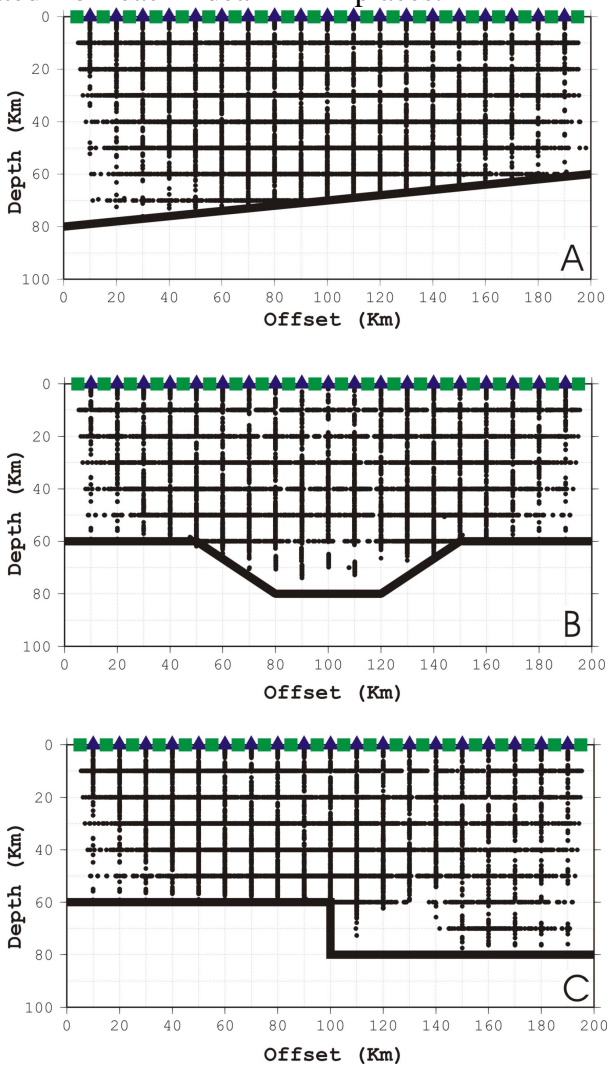

Figure 3. Ray coverage from reflection waves as calculated from the forward modelling. The raypaths of reflected waves are presented by the dots on to the grid lines. Low raypath coverage at the edges and in the area of reflector anomaly is observed due to source-receiver geometry and reflector anomaly.

Figure (4A) shows the tomographic result for the dipping reflector. At the end of third iteration, reflector is reconstructed by 95%.

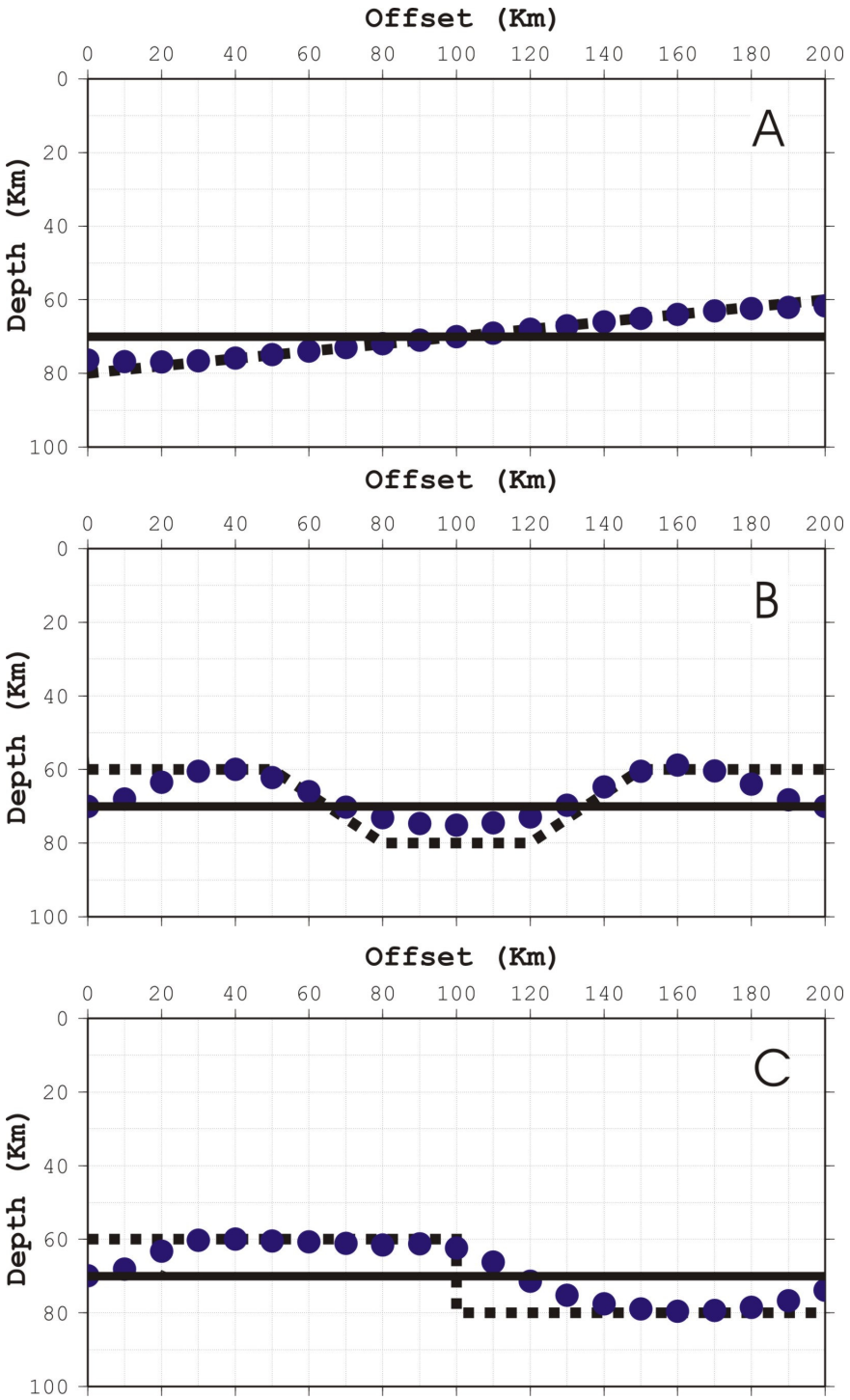

Figure 4. Reconstruction of reflector, by inverting reflection travel times. The ideal reflector is described by dashed line and the continuous line denotes the starting reflector geometry. Solid bullets present the final reflector. A) Dipping layer. The "true" model is reconstructed by 95%, B) Syncline model, which is finally reconstructed by more than 87% and C) Reflector with of a fault-like model, which is poorly reconstructed due to low ray coverage close to the fault region.

Figure (4B) presents the tomographic image in cross section for the syncline model which is useful in the reconstruction of tectonic structures. The results show that reflector geometry is well reconstructed. The reconstructed model shows discrepancies from the actual one at low raypath coverage regions such as the edges and the middle of the model. For the reflector with fault, ranging between the depths of 60 km and 80 km, the algorithm recovers its depth quite well (figure 4C). However, some regions (edge of reflector) were reconstructed poorly, due to low ray coverage (Figure 3C). The r.m.s error was reduced from 28.96 s (initial model consisting of a flat reflector model) to 2.31 s.

Reconstruction of the velocity model and the reflector geometry

The input model is 200 Km long and 100 Km deep, with a background velocity model which consists of four layers, whose velocity increases linearly with depth (equation 15 and table 1) and a flat reflector at a depth of 70 Km. The same velocity anomaly as in figure (1A) with a lower amplitude (10%) and the three initial reflectors of figure (3) are also used for the calculation of critically refracted and reflected waves. We have used a narrow as well as a dense grid with 21/41 nodes in the x direction, 1 in the y direction and 11/21 in the z direction (depth), resulting in a total of 231/861 velocity nodes and 21/41 reflector nodes. 19 sources with 20 geophones along the top of the model were used, thus resulting in 760 (2*380) travel time observations. Figure (5) presents the raypath coverage from the simultaneous solution of the forward problem using first arrivals and reflection traveltimes. Poor ray coverage is also observed in regions near the reflector. Figures (6A), (6B) and (6C) show the inversion results. We should note that contours represent the percentage (%) of the reconstructed velocity model. Thus, the high velocity region is reconstructed quite well, since the rays sample better the faster regions. Regarding the reflector, the inversion recovered its geometry quite well except for the fault model due to low ray coverage. It is important to notice that the main velocity model characteristics, such as the amplitude and shape of the anomalies were better determined than in the previous test.

3D synthetic test for the modelling in complex geological area

The 3D model was defined as 16 Km^2 and 100 Km deep using the same background velocity model as presented in table (1).

Table 1. Starting background velocity model

Layer	Average Velocity (Km/s)	Depth
1	1.075	5
2	2.2	20
3	4.075	45
4	6.7	80

We used almost the same model as in figure (1) with 3D source and receiver geometry. A high velocity anomaly (20%) lying on the top of the flat initial reflector and an ideal reflector like a anticline geological structure are used for the calculation of the synthetics travel times. The initial reflector model was a flat discontinuity at a depth of 60 Km. We have used a narrow 3D grid with 16 nodes in the x direction, 16

nodes in the y direction and 21 in the z direction (depth), resulting in a total of 5376 velocity nodes and 256 reflector nodes. A total number of 21 shot points (triangle) distributed on the top of the model were recorded by 20 surface geophones (square) as is shown in figure (7). The final data set consisted of 840 first breaks of P waves and reflections traveltimes from the initial reflector.

Figure (7) presents in 3D the tomographic image from the simultaneous inversion of first arrivals and reflection traveltimes for the last iteration. The result shows that the initial model is well reconstructed. Applying appropriate regularization parameters has deflected some artefacts. It was interesting that in the area of interest both the amplitude and the shape of anomaly (velocity/reflector) are significantly reconstructed for more than 50%.

CONCLUSION

We present a tomographic method for joint estimation of the velocity field and reflector position using first arrivals and reflection travel-times. We have also shown that our algorithm is capable of producing reliable tomographic images using synthetic data. This method may be also helpful in constructing complex geological models with local bodies, synclines, anticlines and faults. The proposed method is also able to perform an accurate determination of the shallow velocity model and correct the large time shifts (statics) in reflections, resulting in better reflector continuity. Moreover, we can use tomographically determined velocities to image seismic data applying depth migration, avoiding stacking and normal moveout (prestack migration).

The proposed method incorporates the use of an efficient ray tracing technique and a finite difference code for solving the forward problem in conjuction with a combination of inversion stabilization approaches. In spite of the amount of data, the proposed method and algorithm are quite efficient, since they require relative small computation times.

REFERENCES

Aki, K., and W. H. K. Lee, 1976, Determination of three-dimensional velocity anomalies under a seismic array using first p arrival times from local earthquakes: 1, A homogeneous initial model: J. Geophys. Res., **81**, 4381-4399.

Aki, K., Christofferson, A., and Husebye, E. S., 1977, Determination of the three dimensional seismic structure of the lithosphere: J. Geophys. Res., **82**, 277-296.

Anderson, D. L., and Dziewonski, A. M., 1984, Seismic Tomography: Scientific American **251**, No 10, 60-68.

Ammon, C. J., and Vidale, J. E., 1990, Seismic travel-time tomography using combinatorial optimisation techniques: Seis. Res. Lett., **61**, 39.

Bickel S. H., 1990, Velocity-Depth ambiguity of reflection travel-times: Geophysics, **55**, 266-276.

Bishop, T. N., Bube, K. P., Cutler, R. T., Langan, R. T., Love, P. L., Resnick, J. R., Shuey, J. T., Spindler, D. A. and Wyld, H. W., 1985, Tomographic determination

of velocity and depth in laterally - varying media: Geophysics, **50**, 903-923.

Cerveny, V., Soares E. P., 1992, Fresnel volume ray tracing: Geophysics, **57**, 902-915.

Constable, S. C., Parker, R. L., and C. Constable, 1987, Occam's inversion: A practical algorithm for generating smooth models from electromagnetic sounding data: Geophysics, **52**, 289-300.

Farra, V. and Madariaga, R., 1988, Non-linear reflection tomography: Geophysics. J., **95**, 135-147.

Franklin, J. N., 1970, Well-posed stochastic extension of ill-posed linear problems: J. Math. Anal. Appl., **31**, 682-716.

Hobro, J.W.D., Singh, S.C. and Minshull, T.A., 2003, Three-dimensional tomographic inversion of combined reflection and refraction seismic traveltime data: Geophysical Journal International, 152, 79-93.

Hole, J. A., and Zelt, B. C., 1995, 3-D finite-difference reflection travel-times: Geophys. J. Int., **121**, 427-434.

Lanczos, C., 1950, An iteration method for the solution of the eigenvalue problem of linear differential and integral operators: J. Res. Nat. Bur. Stand., **45**, 255-82.

Lees, J. M., and Crosson, R. S., 1989, Tomographic inversion for three dimensional velocity structure at Mount St. Helens using Earthquake data: JGR, **94**, B5, 5716-5728.

Levenberg, K., 1944, A method for the solution of certain nonlinear problems in least-squares: Quart. Appl. Math., **2**, 164-168.

Lines, L., 1993, Ambiguity in analysis of velocity and depth: Geophysics, **58**, 596-597.

Marquardt, D. W., 1963, An algorithm for least-squares estimation of nonlinear parameters: Soc. Industr. Appl. Math., J. Appl. Math., **11**, 431-441.

Moser, T. J., Nolet, G. and Snieder, R., 1992, Ray Bending Revisited: Bulletin of the Seismological Society of America, **82**, 259-288.

Officer, C. B., 1958, Introduction to the Theory of Sound Transmission: McGraw-Hill, New York, pp. 284.

Paige, C. C., and Saunders, M. A., 1982, LSQR: An algorithm for sparse linear equations and sparse least squares: A.C.M. Trans. Math. Software., **8**, 43-71.

Papazachos, C.B., and Nolet, G., 1997, P and S deep velocity structure of Hellenic area obtained by robust non-linear inversion of arrival times: J. Geophys. Res., **102**, 8349-8367.

Pereyra, V., 1992, Two-point ray tracing in general 3D media: Geophysical Prospecting, **40**, 267-287.

Podvin, P. and Lecomte, I., 1991, Finite difference computation of travel-times in very contrasted velocity models: a massively parallel approach and its associated tools: Geophys. J. Int., **105**, 271-284.

Press, W. H., B. P. Flannery, S. A. Teukolsky, and W. T. Vetterling, 1988, Numerical Recipes in Fortran - The Art of Scientific Computing: Cambridge University Press, Cambridge, pp. 292, 305-309.

Ross, W. S., 1994, The velocity-depth ambiguity in seismic travel-time data, Geophysics, **59**, 830-843.

Soupios, P.M., Papazachos, C.B, Juhlin, C., Tsokas, G.N., 2001, Non-linear three-dimensional travel-time inversion of crosshole data with an application in the area of

middle Urals, Geophysics, **66**, 627-636.

Soupios, P.M., 2002, Implemenation of tomographical Methods for the Determination of Geotechnical Parameters in the Bridge of Nestos River: Technical Report, 145 pp (in Greek).

Stork, C. and Clayton, R. W., 1986, Analysis of the resolution between ambiguous velocity and reflector position for travel-time tomography: Extended Abstracts of the 56th SEG International Meeting, 545-550.

Tarantola, A., 1987, Inverse Problem Theory: Elsevier, Amsterdam.

Tarantola, A., and A. Nercessian, 1984, Three-dimensional inversion without blocks: Geophys. J. R. Astr. Soc., **79**, pp. 299-306.

Thurber, C. H., 1983, Earthquake locations and three-dimensional crustal structure in the Coyote lake area, Central California, J. Geophys. Res., **88**, 8226-8236.

Thurber, C. H., and Ellsworth, W. L., 1980, Rapid solution of ray tracing problems in heterogeneous media: Bulletin of the Seismological Society of America, **70**, 1137-1148.

Tieman, H. J., 1994, Investigating the velocity-depth ambiguity of reflection travel-times: Geophysics, 59, 1763-1773.

Trinks, I, Singh, S. C., Chapman, C. H., Barton, P. J., Bosch, M. and Cherrett, A., 2005, Adaptive traveltime tomography of densely sampled seismic data: Geophysical Journal International, **160**, 925-938.

Wielandt, E., 1987, On the validity of the ray approximation for interpreting delay times: Seismic Tomography (Guust Nolet), D. Reidel Publishing Company.

Williamson, P. R., 1990, Tomographic inversion in reflection seismology, Geophys. J. Int., **100**, 255-274.

Woodward, M. J., 1992, Wave-equation tomography: Geophysics, **57**, 15-26.

Zelt, C. A., A. M. Hojka, E. R. Flueh, and K. D. McIntosh, 1999, 3D simultaneous seismic refraction and reflection tomography of wide-angle data from the Central Chilean margin: Geophys. Res. Lett., **26**, 2577-2580.

Zhang, J., U.S. ten Brink, M. N., Toksoz, 1998, Nonlinear refraction and reflection travel-time tomography: JGR-Solid Earth, **103**, B12, 729-743.